Journal of Materials Chemistry A

RSC Publishing

PAPER

View Article Online
View Journal | View Issue

Cite this: J. Mater. Chem. A, 2013, 1, 611

Atomically precise silver clusters for efficient chlorocarbon degradation†

M. S. Bootharaju,‡ G. K. Deepesh,‡ T. Udayabhaskararao and T. Pradeep*

We describe the degradation of chlorocarbons (CCl_4, $C_6H_5CH_2Cl$ and $CHCl_3$) in solution at room temperature (27 ± 4 °C) by the monolayer-protected silver quantum cluster, Ag_9MSA_7 (MSA: mercaptosuccinic acid) in the presence of isopropyl alcohol (IPA). The main degradation products were silver chloride and amorphous carbon. Benzyl chloride was less reactive towards clusters than CCl_4 and $CHCl_3$. Materials used in the reactions and the reaction products were characterized using several spectroscopic and microscopic tools such as ultraviolet-visible (UV/Vis) absorption spectroscopy, Fourier transform infrared spectroscopy (FTIR), photoluminescence spectroscopy, X-ray diffraction (XRD), Raman spectroscopy, X-ray photoelectron spectroscopy (XPS), energy dispersive analysis of X-rays (EDAX) and scanning electron microscopy (SEM). We have shown that clusters are more efficient for the degradation of halocarbons than the corresponding monolayer-protected nanoparticles (Ag@MSA, particle diameter 15 ± 5 nm) at a given time and temperature. The higher reactivity of clusters is attributed to their small size and large surface area. Clusters and nanoparticles were used for reactions in supported (on neutral alumina) and unsupported forms. A possible mechanism for the reaction has been postulated on the basis of experimental results.

Received 10th September 2012
Accepted 12th October 2012

DOI: 10.1039/c2ta00254j

www.rsc.org/MaterialsA

Introduction

Research on noble metal (silver and gold) quantum clusters[1,2] has become increasingly fascinating in the last two decades. Quantum clusters, composed of a few tens to hundreds of atoms at the core and protected with ligands, are the connecting link between nanoparticles and molecules which exhibit molecular optical properties like absorption,[3,4] emission,[5,6] chirality,[7] *etc.* These nanosystems are very interesting because they show several applications in various fields such as catalysis,[8,9] biology,[10] environmental remediation,[11] *etc.* They are highly reactive due to their extremely small size and large surface area. They show unusual reactivity with salts.[12] Metal clusters exhibit the property of alloying with other metals.[13,14] Clusters have been used for sensing metal ions[15–17] and anions[18] by using their luminescence property.

The environment has been contaminated by a large number of pollutants like organic halides[19] (chloroflurocarbons (CFC), C_2Cl_4, C_2ClF_3, CCl_4, *etc.*), heavy metals[20] (Hg, Pb, Cd, Cr, *etc.* in various forms), energetic materials[21] (hexahydro-1,3,5-trinitro-1,3,5-triazine (RDX) and 2,4,6-trinitrotoluene (TNT)), and many others. Halocarbons are harmful trace components in water and air, either in the context of biological toxicity or due to their global warming potential or undesirable atmospheric chemistry.[22] The main sources of these are cleaning solvents, lubricants, plasticizers and refrigerants. Several of these have been replaced by less harmful chemicals. However, many of them continue to be used due to economic considerations or the lack of suitable replacements. CCl_4 is a widely used solvent in industry, research laboratories, dry cleaning, *etc.*[23] It is carcinogenic and it can persist in ground and surface waters. Due to this, it is one of the complex contaminants. The maximum allowed level of CCl_4 in surface water is 5 μg L^{-1}.[24] CFCs cause depletion of the ozone layer.[25] Various methods such as photodecomposition,[26] incineration,[27] photocatalysis[28,29] and adsorption[30] are developed to eliminate halocarbons from the environment. Chlorinated halocarbons are degraded by reductive mechanisms.[31] There are four types of reductive mechanisms: hydrogenolysis, elimination, dehydrohalogenation and hydrogenation.

Nanoparticles are increasingly used for environmental applications due to increased amount of contaminants in soil and groundwater.[32] Common nanoparticles used for halocarbon degradation in the literature are iron in oxide and zero-valent forms,[31] MgO[33] and ZnO.[34] In most of the above studies, nanoparticles form corresponding metal halides as principal products at high temperatures. Recently, noble metal and oxide nanoparticles have been studied in the degradation of

DST Unit of Nanoscience (DST UNS), Department of Chemistry, Indian Institute of Technology Madras, Chennai - 600 036, India. E-mail: pradeep@iitm.ac.in

† Electronic supplementary information (ESI) available: SEM elemental analysis and photograph of supported silver clusters, UV/Vis absorption spectrum and TEM image of Ag@MSA nanoparticles, XPS, XRD, Raman and EDAX data of the products of the reaction between supported clusters and CCl_4. See DOI: 10.1039/c2ta00254j

‡ These authors have contributed equally.

halocarbons.[35] Our research group has pioneered the use of noble metal nanoparticles for the removal of pesticides and halocarbons from drinking water.[36–40]

The standard Gibbs free energy change of formation ($\Delta_f G^0$) of AgCl(s) and CCl_4(l) are −109.8 and −65.2 kJ mol^{-1}, respectively. The net free energy change for the reaction 4Ag(s) + CCl_4(l) → 4AgCl(s) + C (graphite) is −374.0 kJ mol^{-1}. This indicates that the above reaction is feasible at 298 K and 1 atm pressure. The cell electromotive force (emf), E^0_{cell}, for the reduction of CCl_4 by silver (in the above reaction) is calculated to be 0.97 V using the equation $\Delta_f G^0 = -4FE^0_{cell}$, where F is Faraday's constant (96 500 C or J/V). The reaction may be slow but it is feasible. However, by using materials at the nanoscale, particularly silver at the nano/cluster length scale, the reduction potential is expected to reduce significantly as nanoscale silver is metastable with respect to the bulk. Due to the reduced dimension, the reaction is likely to be kinetically more favorable. Therefore, we may see interesting reactivity. This motivated us to study the reaction of CCl_4 with silver quantum clusters.

In the context of environmental applications, there are only a few studies on metal clusters. A study of sensitivity of Au_{25} clusters, one of the most studied clusters, to various metal ions was performed by Habeeb Muhammed and Pradeep.[12] Subsequently, a number of studies have shown the effect of metal ions on monolayer-protected as well as protein-protected gold clusters.[10,15,41] Sensing experiments have been performed with silver clusters as well.[16,17] There is a large need to develop techniques to use such materials as commercial products. Here, we utilized Ag_9 clusters protected with mercaptosuccinic acid (MSA) for the complete catalytic degradation of CCl_4, $CHCl_3$ and $C_6H_5CH_2Cl$ at room temperature. The reaction products were AgCl, CCl_3COOH, amorphous carbon and acetone. We found that isopropyl alcohol (IPA), used to increase the solubility of halocarbons in water, is very important in the reaction. Mechanistic aspects of the reaction are discussed based on experimental results. We propose that Cl^- ions, which are formed due to the cleavage of Cl_3C–Cl, replace the thiolates on the surface of the cluster. As a result, stability of the cluster is lost which causes the interaction of silver with Cl^-, leading to the formation of AgCl. The detached thiolates are converted to stable sulphites/sulphates in solution, the presence of which was confirmed by XPS. We demonstrate the increased efficiency of clusters for halocarbon degradation compared to analogous MSA protected silver nanoparticles. Reactions were carried out with clusters supported on alumina also, in which observations similar to unsupported clusters were noted.

Experimental section

Materials

Silver nitrate (CDH, India), mercaptosuccinic acid (MSA), sodium borohydride (Sigma Aldrich), methanol, ethanol, isopropyl alcohol (IPA), carbon tetrachloride (CCl_4), benzyl chloride ($C_6H_5CH_2Cl$) and chloroform ($CHCl_3$) (SRL Chemical Co. Ltd., India) were purchased from various sources and used as such without further purification. Neutral alumina was supplied by SRL, India. The surface area and the mean particle size were 900 ± 50 cm^2 g^{-1} and 0.13 mm, respectively.

Synthesis of silver clusters

The Ag_9MSA_7 cluster was synthesized according to the reported protocol.[42] Briefly, 47 mg of $AgNO_3$(s) and 187 mg of MSA(s) were ground until the mixture turned orange due to the formation of Ag-thiolates. After that, about 50 mg of $NaBH_4$(s) was added to it and grinding was continued for 2–3 minutes. To this, 10 mL of distilled water was added which led to the formation of clusters. The cluster was precipitated by the addition of ethanol. The precipitate was washed several times with pure methanol to remove excess $NaBH_4$, MSA and thiolates. Finally, a reddish brown powder of the clusters was obtained after evaporation of methanol using a rotavapor.

Synthesis of Ag@MSA nanoparticles

Ag@MSA nanoparticles were prepared as per the previous report.[20] Nearly 1.7 mL of distilled water containing 85 mg of $AgNO_3$ was added to 100 mL of methanol containing 448.9 mg of MSA which was kept at 0–5 °C. The resulting solution was stirred at 4000 rpm. 25 mL of freshly prepared 0.2 M $NaBH_4$ solution was added to the above solution drop-wise. Stirring was continued for 45 minutes at 0–5 °C. The mixture containing the precipitate of nanoparticles was centrifuged and the residue was washed with methanol to remove excess MSA and $NaBH_4$. Finally, a black powder of nanoparticles was obtained by evaporating methanol using a rotavapor.

Preparation of supported clusters and nanoparticles on neutral alumina

Loading of clusters was done by the addition of cluster solution (known amount) to a calculated amount of alumina followed by shaking with a mechanical shaker. The color of the solution disappeared immediately, indicating adsorption of clusters on alumina. The addition of cluster solution and shaking were continued until the supernatant retained the color of the cluster solution, indicating saturation loading. The supernatant at this stage showed the absorption features of the clusters, indicating the saturation of the alumina surface with adsorbed clusters. The saturation limit was found to be 10 mg per gram of alumina. After surface saturation, the supernatant was removed by centrifugation. Supported clusters were washed with water followed by methanol to remove the excess cluster. A solvent-free material was obtained by evaporation using a rotavapor. The same method was followed to prepare Ag@MSA nanoparticles supported on neutral alumina.

Reaction of halocarbons with clusters and nanoparticles

Nearly 5 mL of CCl_4 was added to the cluster solution (25 mg in 30 mL water). To this, 10 mL of isopropyl alcohol (IPA) was added. Here, the importance of IPA was to increase the miscibility of CCl_4 in the reaction mixture (solubility of CCl_4 = 800 mg L^{-1} in water at 298 K). The above mixture (orange red color) was stirred at 4000 rpm for 24 h at room temperature. The CCl_4 layer

disappeared and a grey colored precipitate was formed after 1.5 h. These observations indicate the occurrence of reaction between clusters and CCl_4. Reactions were carried out in methanol and ethanol as well in place of IPA. In these cases, no reaction was seen. A probable reason is that oxidation of IPA is more facile than other alcohols (methanol and ethanol). Other halocarbons, $CHCl_3$ and $C_6H_5CH_2Cl$, were used in place of CCl_4 under identical experimental conditions. A precipitate was formed after 24 h in the case of benzyl chloride, indicating less reactivity. In the case of supported clusters, 500 mg of the material was used under the above experimental conditions. Similar quantities of Ag@MSA nanoparticles (both unsupported and supported) were also used for the reaction of halocarbons.

Instrumentation

UV/Vis absorption spectra were recorded with a PerkinElmer Lambda 25 instrument in the spectral range of 200 to 1100 nm. FTIR spectra were recorded with a PerkinElmer Spectrum One instrument. KBr crystals were used as the matrix for preparing the samples. X-ray photoelectron spectroscopy (XPS) measurements were done using an Omicron ESCA Probe spectrometer with polychromatic Mg Kα X-rays ($h\nu = 1253.6$ eV). Experiments were carried out at an X-ray power of 300 W and pass energies of 50 eV for survey scans and 20 eV for specific regions. The base pressure of the instrument was 5.0×10^{-10} mbar. The binding energy was calibrated with respect to the adventitious C 1s feature at 285.0 eV. Most of the spectra were deconvoluted to their component peaks using the software CASA XPS. Scanning electron microscopy (SEM) and energy dispersive analysis of X-rays (EDAX) were performed using a FEI QUANTA-200 SEM. For the SEM measurements, samples were spotted on an indium tin oxide (ITO)-coated conducting glass and dried in ambience. X-ray diffraction (XRD) data were collected with a Shimadzu XD-D1 diffractometer using Cu Kα ($\lambda = 1.54$ Å) radiation. The samples were scanned in the 2θ range of 10 to 90°. The electrospray ionization mass spectrometry (ESI MS) measurements were done in the negative and positive modes using a MDX Sciex 3200 QTRAP MS/MS instrument having a mass range of m/z 50–1700, in which the spray and the extraction are orthogonal to each other. The samples were electrosprayed at a flow rate of 10 μL min^{-1} and an ion spray voltage of 5 kV. The spectra were averaged for 100 scans. MS/MS spectra were collected at optimized collision energies in the range of 25–45 eV.

Results and discussion

Starting materials: clusters, nanoparticles and supported materials

Silver nanoclusters (Ag_9MSA_7) and Ag@MSA nanoparticles have been well characterized as per other reports[20,42] and we present here only the essential data. As-synthesized silver clusters show characteristic UV/Vis absorption features at 450, 490, 626 and 886 nm (Fig. 1A). These clusters showed red emission at 726 nm when excited at 590 nm in a water–methanol mixture at 5 °C (inset of Fig. 1A). These two data prove the formation of clusters. The evidence for the binding of MSA to the cluster core was obtained by FTIR analysis (Fig. 1B). Pure MSA shows a characteristic –CO– of free carboxylate and S–H stretching peaks at 1700 and 2566 cm^{-1}, respectively (trace (a)). In the cluster sample, carboxylate stretching mode got shifted to 1576 cm^{-1} and the S–H stretching peak was absent (trace (b)). The presence of characteristic peaks of MSA in clusters (trace (b)) with a characteristic shift in peak positions in comparison to parent MSA (trace (a)) confirms the binding of MSA. The absence of the S–H feature (marked in trace (a)) in the cluster sample shows the binding of MSA with the cluster through an Ag–S linkage.[42] The chemical nature of silver and sulphur was confirmed by XPS (discussed later).

Supported clusters on alumina were characterized by SEM EDAX and the data are shown in Fig. S1 of ESI.† The spectrum

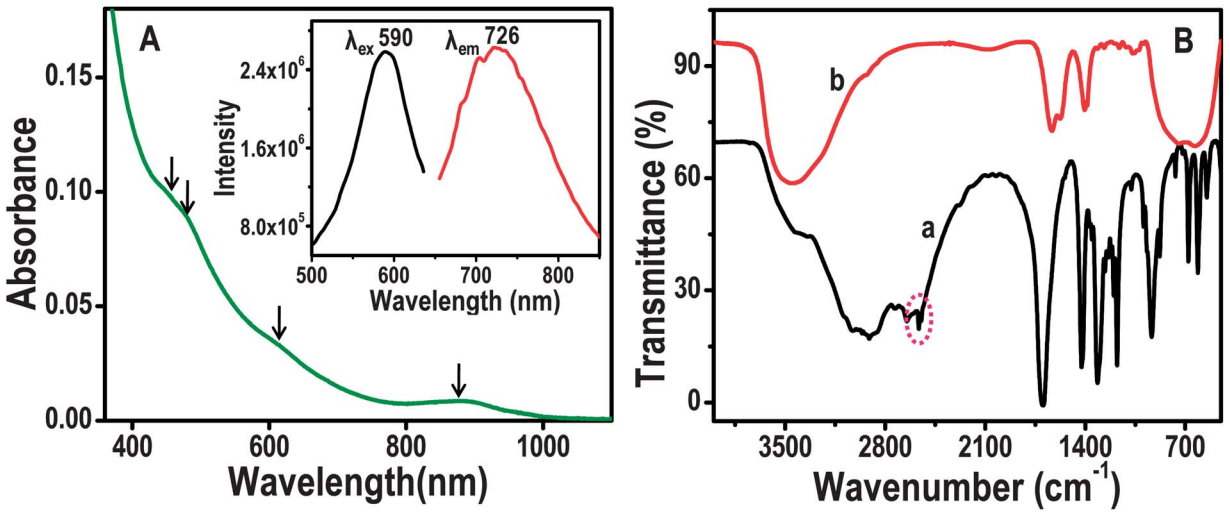

Fig. 1 (A) UV/Vis absorption spectrum of as-synthesized Ag_9MSA_7 clusters. Inset of (A) is the photoluminescence excitation and emission spectra of the clusters. They show emission at 726 nm when excited at 590 nm, at 5 °C. (B) Comparison of the FTIR spectra of MSA and Ag_9MSA_7 (traces (a) and (b), respectively); the latter shows the absence of S–H stretching in (b).

shows the presence of elements silver and sulphur which confirms the adsorption of clusters. Important evidence to show the presence of clusters on alumina is the red luminescence of the supported cluster kept under a UV lamp at liquid nitrogen temperature (inset of Fig. S1†). Bare alumina does not show any luminescence under UV lamp. The Ag@MSA nanoparticles were characterized by absorption spectroscopy. Silver nanoparticles show a surface plasmon resonance band at 392 nm which proves the formation of nanoparticles (Fig. S2†). TEM analysis of nanoparticles shows the average size to be 15 ± 5 nm (inset of Fig. S2†).

Reaction with CCl_4

We performed reactions with unsupported and supported clusters (on alumina) which are presented separately.

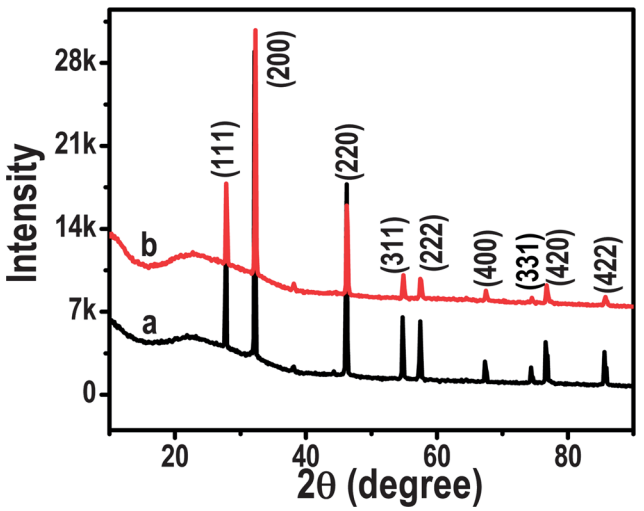

Fig. 2 XRD of as-prepared AgCl (a) and the product (b) obtained due to the reaction of Ag_9MSA_7 with CCl_4. The data have not been corrected for the background.

A. Unsupported clusters. The reactions were performed as described in the Experimental section. We have products in the solid state and products in solution. While the former are studied by XRD, Raman, IR, *etc.*, the latter are studied by mass spectrometry. The grey colored precipitate and colorless supernatant obtained after the reaction of CCl_4 and clusters were characterized with various analytical tools. The XRD pattern of the precipitate is shown in Fig. 2. It matches exactly with as-prepared AgCl (a precipitate obtained after mixing solutions of $AgNO_3$ and NaCl). This observation confirms the formation of AgCl as the reaction product.

The precipitate was used for Raman analysis before and after washing with ammonia solution (Fig. 3A). The purpose of washing with ammonia was to remove AgCl as a soluble complex, $[Ag(NH_3)_2]^+Cl^-$. After that, the solution was centrifuged at 10 000 rpm. A black residue was obtained which was analyzed by Raman spectroscopy. The unwashed precipitate (trace (a)) shows the presence of peaks at ~1408 and ~1575 cm^{-1}. These are attributed to D and G bands of carbonaceous species which is due to the formation of carbon from degradation of CCl_4.[43] After washing with ammonia, the peaks got shifted to ~1357 and ~1590 cm^{-1} (trace (b)). This shift may be due to the removal of impurities like AgCl which are soluble in ammonia. The red shift of the D band may be due to variation in defects (due to washing with NH_3 solution) of the graphitic structure and the blue shift of the G band is due to further amorphization of carbon due to removal of impurities.[44] Comparison of FTIR data of the reaction product (Fig. 3B) and the parent cluster (trace (a) in the inset of Fig. 3B) further supports the formation of the carbonaceous material. The stretching modes of the carboxylate group at 1576 and 1407 cm^{-1} are completely absent in the reaction product (trace (b) in the inset of Fig. 3B). This confirms the removal of a monolayer of MSA from the cluster. The peak at 1625 cm^{-1} in traces (a) and (b) is due to adsorbed water. A strong peak at 1384 cm^{-1} has emerged due to the presence of carbonaceous

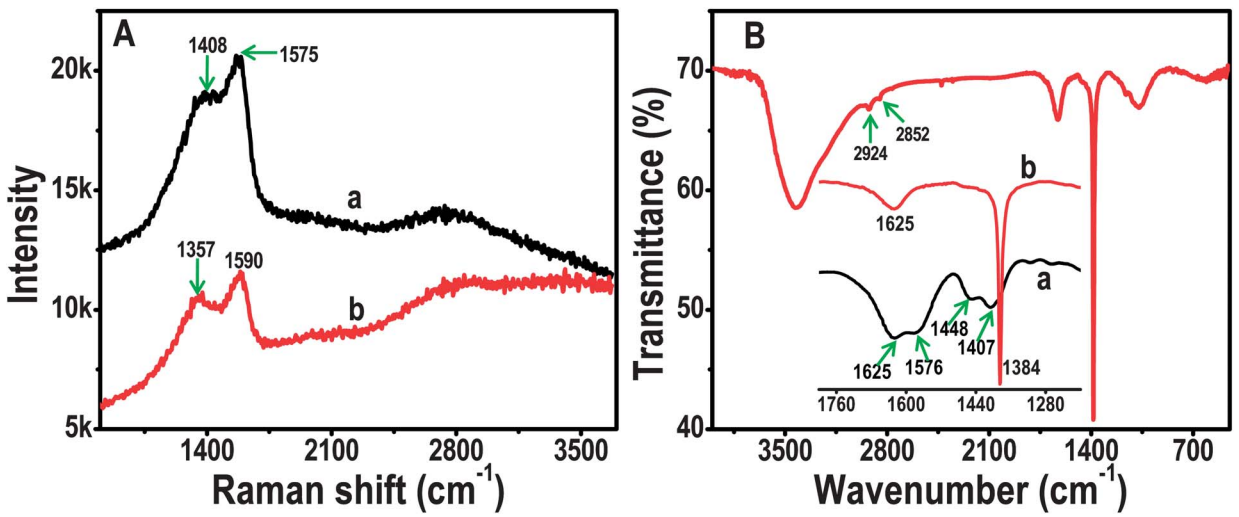

Fig. 3 (A) Raman spectra of the reaction product of Ag_9MSA_7 and CCl_4 before and after washing ((a) and (b), respectively) with aqueous ammonia. (B) FTIR spectrum of the reaction product before washing. Inset of (B) is the FTIR spectra of parent clusters (a) and the reaction product (b) in a specific region.

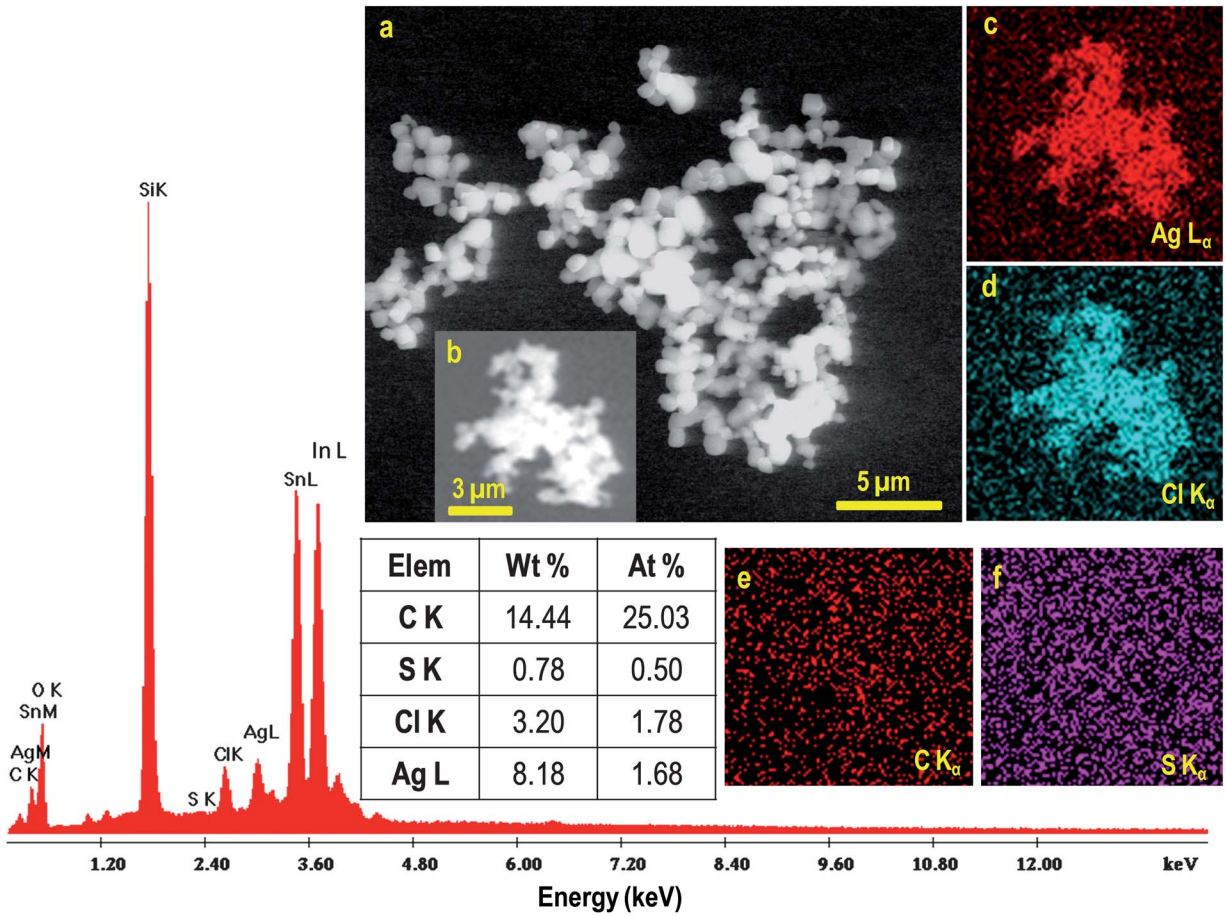

Elem	Wt %	At %
C K	14.44	25.03
S K	0.78	0.50
Cl K	3.20	1.78
Ag L	8.18	1.68

Fig. 4 EDAX spectrum of the product obtained after the reaction of the Ag_9MSA_7 cluster with CCl_4. The quantification table of elements in the EDAX spectrum is also shown. Si, In and Sn are due to the indium tin oxide substrate used. (a) and (b) are SEM images of the above sample. Elements Ag, Cl, C and S of the region shown in (b) are mapped in (c)–(f), respectively using X-ray energies of Ag L_α, Cl K_α, C K_α and S K_α.

species which confirms the formation of carbon, possibly as a graphitic product.[45] The other peaks at 2924 and 2852 cm^{-1} in Fig. 3B are due to the C–H stretching mode in graphitic carbon. The presence of chemically transformed sulphur species (sulphite/suphate) which are adsorbed on the reaction product and the absence of carboxylate features were confirmed by XPS (discussed later). From all these, it is evident that a monolayer of the cluster has been transformed chemically. However, the mechanism is complex and is not understood well.

SEM analysis of the precipitate is given in Fig. 4. Fig. 4a is a large area SEM image. It shows the presence of AgCl crystals. The elemental maps of the area shown in (b) are presented in (c)–(f). They clearly show the presence of elements Ag, Cl and a little amount of C. The EDAX spectrum collected from a portion of the sample is shown in Fig. 4. It shows the presence of elements Ag, Cl and trace amounts of S. The quantification table of elements of the same area (in Fig. 4) shows the presence of Ag and Cl in 1 : 1 atomic ratio which matches with AgCl composition. Also it shows the atomic percent of C and S in which sulphur was seen less in quantity.

In Fig. 5, XPS data of the precipitate (traces (b)) are compared with parent silver clusters (traces (a)). In the survey spectra of both the samples, carbon, silver, sulphur and oxygen were present (Fig. 5A). After the reaction, a new peak around 200.0 eV appears due to the presence of chlorine. The C 1s regions of the cluster and the reaction product clearly indicate the almost complete disappearance of the peak at 288.9 eV due to the carboxylate[46] groups in the product (Fig. S3†). This observation is also supported by FTIR analysis which confirms the replacement of the ligand MSA on the cluster. The intensity of the peak at 286.5 eV (due to carbon in C–O) increased compared to the parent clusters. The Ag 3d regions of both the samples are compared in Fig. 5B. Before the reaction, Ag $3d_{5/2}$ appeared at 368.1 eV whereas it is at 367.6 eV after the reaction. This clearly reveals the oxidation of silver from Ag^0 to Ag^+ state.[16] Note that in Ag, oxidation leads to shifting of binding energy to lower values.[16] The S 2p region due to the monolayer of the cluster is shown in Fig. 5C. Before the reaction, S $2p_{3/2}$ was at 162.1 eV assigned to sulphur bound to the cluster in the thiolate form. After the reaction, it shifted to 168.5 eV. This suggests the chemical change of the monolayer due to the reaction of the cluster core. This peak is assigned to sulphate/sulphite species.[47] The Cl 2p feature (Fig. 5D) is quite broad and it is fitted into two components corresponding to two types of Cl moieties. The Cl $2p_{3/2}$ positions are at 198.9 and 201.1 eV. The former peak may be due to chemisorbed chloride[48] possibly

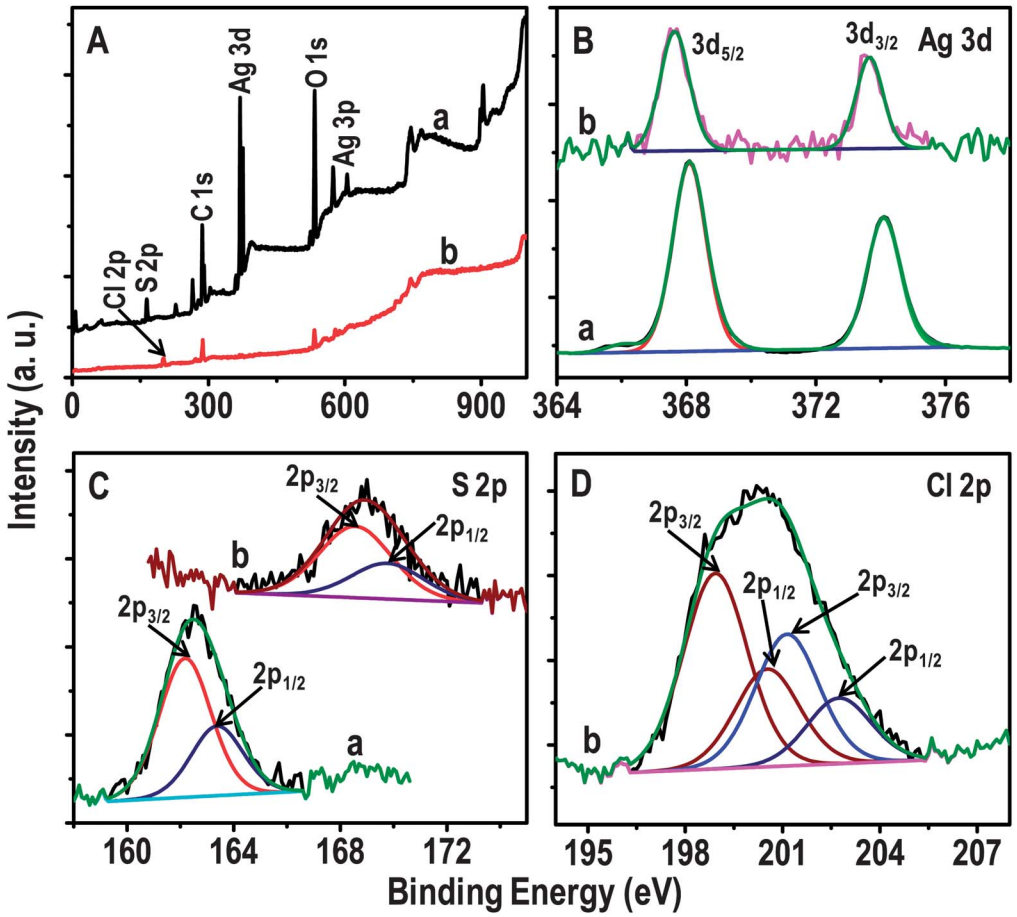

Fig. 5 XPS of parent Ag_9MSA_7 clusters (a) and the product obtained after the reaction of clusters with CCl_4 (b). (A–D) survey spectra, Ag 3d, S 2p and Cl 2p regions, respectively.

from AgCl and the latter may be due to adsorbed organic chlorine, possibly from CCl_4.[39,49] While all the silver got reacted in this sample, there could be some CCl_4 left behind.

During the progress of the reaction, we have followed the variation in pH of the solution with time (Fig. 6A). Initially, the pH of the reaction mixture was 5.7. The pH after 1.0, 2.0, 3.0 and

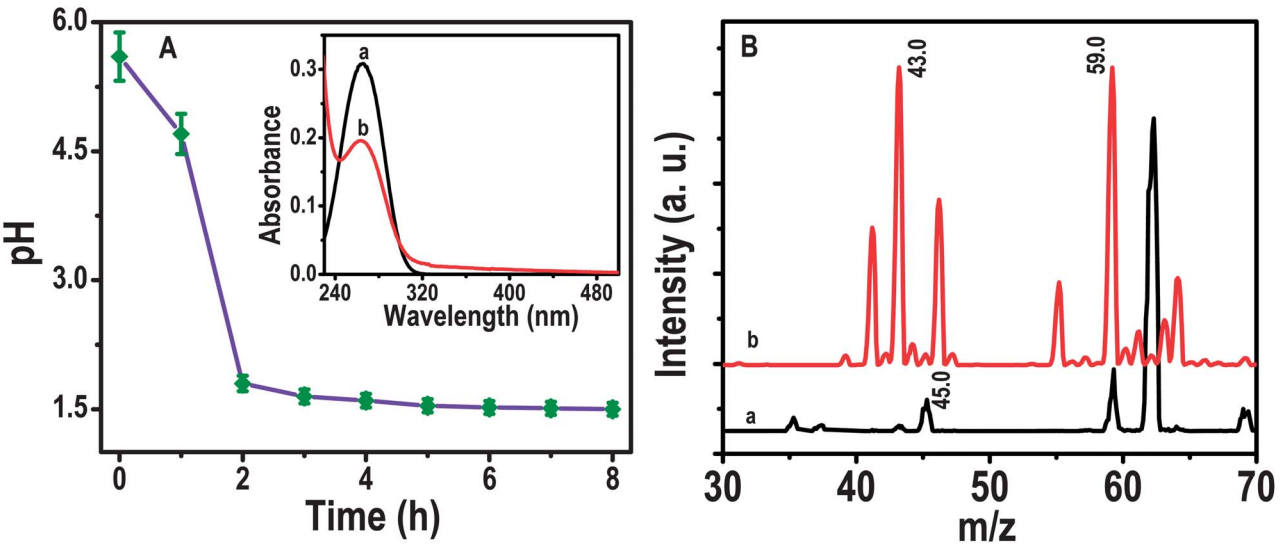

Fig. 6 (A) Plot of pH of the reaction product of Ag_9MSA_7 + CCl_4 with time. The estimated error is 5%. Inset is the absorption spectra of pure acetone (a) and that of the supernatant (b) of the above reaction, after 8.0 h. (B) Comparison of positive mode ESI MS of IPA and the reaction mixture (traces (a) and (b), respectively).

4.0 h of the reaction was 4.7, 1.8, 1.6 and 1.5, respectively. This clearly indicates the increase in the acidity of the reaction mixture. The release of H^+ can be due to the oxidation of IPA to acetone during the reaction. The UV/Vis absorption spectra of the supernatant of the reaction mixture and of acetone are compared in the inset of Fig. 6A. Pure acetone (trace (a)) shows an absorption maximum in water at 265 nm due to n–π* transition of the carbonyl group. The presence of an identical peak at 265 nm (trace (b)) in the reaction mixture confirms the formation of acetone from IPA.[50] Formation of acetone was further confirmed by comparison of ESI MS of IPA and reaction products in solution (Fig. 6B). IPA (trace (a)) shows an intense peak at *m*/*z* 45.0 which is assigned to $CH_3C(OH)H^+$. The reaction product (trace (b)) shows the disappearance of the peak at *m*/*z* 45.0 (due to IPA) with the appearance of a new peak at *m*/*z* 43.0 assigned to CH_3CO^+. The molecular ion peak of acetone was also seen at *m*/*z* 59.0. Interestingly, ESI MS data (Fig. S4†) of the reaction product show the formation of CCl_3COO^- which was tentatively assigned using mass spectrometry/mass spectrometry (MS/MS) analysis. In Fig. S4A,† trace (a) is the positive mode ESI MS of the reaction mixture in which no MSA peak at *m*/*z* 151.0 was noticed. Trace (b) is in negative mode where the peaks at *m*/*z* 196.0 and 161.0 are seen. The MSA peak at *m*/*z* 149.0 was not noticed here as well. The absence of parent MSA peaks after the reaction indicates the chemical transformation of detached ligands. The peak at *m*/*z* 196.0 is assigned to CCl_4COO^-. MS/MS of *m*/*z* 196.0 gives the peak *m*/*z* 161.0 due to the loss of ^{35}Cl (Fig. S4B†). MS^2 of *m*/*z* 198.0 gives 161.0 and 163.0 due to the loss of ^{37}Cl and ^{35}Cl, respectively. Similar losses were seen in MS^2 of *m*/*z* 200.0 and 202.0. The species CCl_4COO^- (or $[CCl_3COO]Cl^-$) may be formed by halogen attachment to CCl_3COO^-. Above assignments were again checked by comparing the calculated and experimental mass spectra for the above species which show an exact match (Fig. S4C and D†). Formation of CCl_3COO^- may be explained as follows. Oxidation of acetone may be continued to form CH_3COOH by active Cl species formed in the reaction (active Cl species can act as oxidizing agents) followed by the formation of chlorinated acid. However, more studies are essential to understand the formation mechanism of such species. A possible chemical equation for the above reaction can be written as follows. The changes observed in the monolayer are not included in the reaction as we do not know the exact mechanism of the chemical transformation of the ligand.

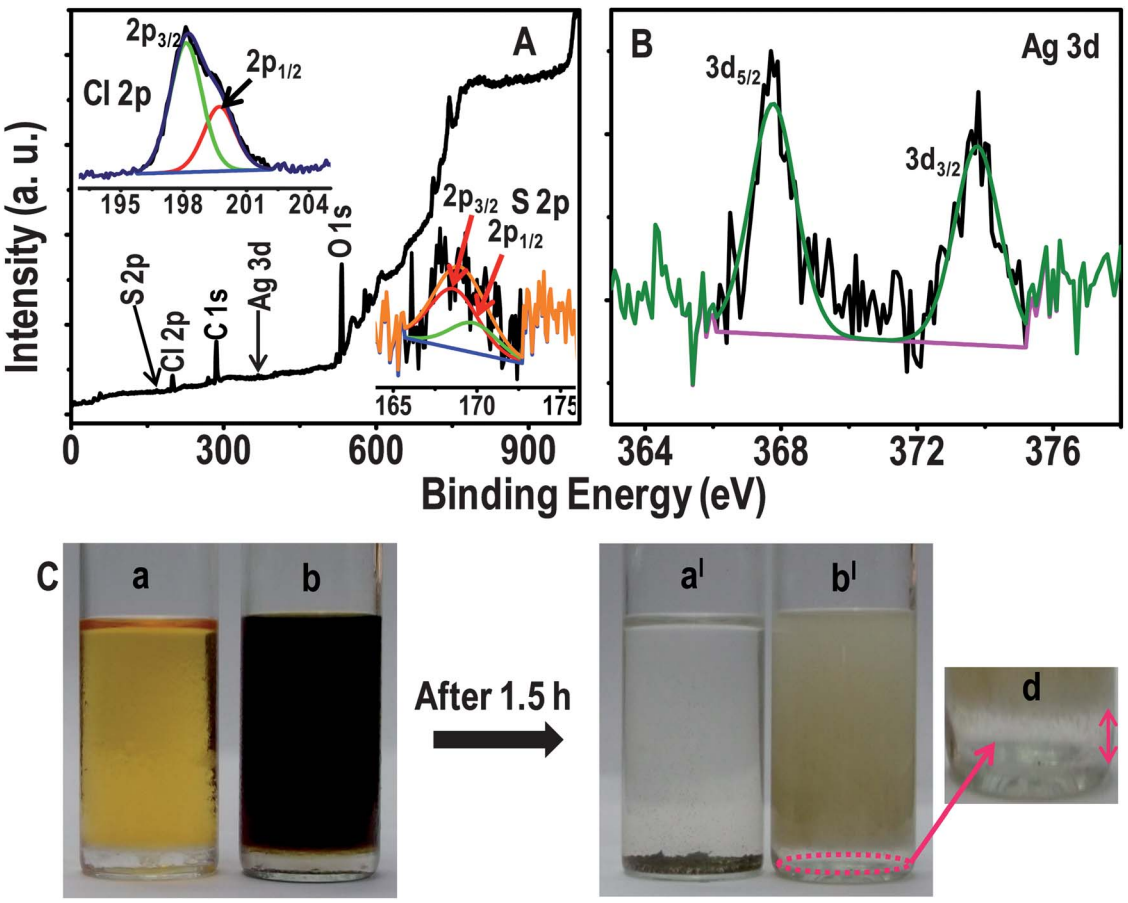

Fig. 7 (A) and (B) XPS survey spectrum and expanded Ag 3d region, respectively of the product of the reaction between Ag_9MSA_7 and benzyl chloride. Insets of (A) are Cl 2p and S 2p regions in the XPS of the same sample. (C) Photographs of the reaction mixtures of (a) Ag_9MSA_7 + CCl_4 and (b) Ag@MSA nanoparticles + CCl_4 initially (0.0 h). The CCl_4 layer is seen separately at the bottom. Photographs (a^I) and (b^I) are of corresponding mixtures after the reaction for 1.5 h. Unreacted CCl_4 is marked in (b^I). An enlarged photograph of the marked area of (b^I) is shown in (d).

Table 1 Comparison of various nanomaterials used for the degradation of chlorocarbons

Nanomaterials	Halocarbons	Process	Conditions	Products	Remarks	Ref.
Elemental iron and zinc	CCl_4	Reductive dechlorination	Ambient conditions	Free metal ions, $CHCl_3$ and H_2	Kinetics depends on pH, surface area, *etc.*	51
Pd/C, Rh/C, Ru/C and Pt/C	Polychlorinated biphenyls (PCBs)	Catalytic dechlorination	2-Propanol, aq. NaOH, 82 °C	Biphenyl and phenylcyclohexane	Complete dechlorination in ~2–3 h	52
TiO_2 (30 nm) suspension	$CHCl_3$, $CHBr_3$, and CCl_3COO^-	Photocatalysis	pH > 11, H_2O + CH_3OH	CO, CO_2 and Cl^-	Xe arc lamp at 910 W, 2 h irradiation	53
Subcolloidal Fe/Ag particles (<0.1 μm size)	Hexachlorobenzene (HCB)	Reductive dehalogenation	Room temperature, in water	Tetra-, tri-, and dichlorobenzenes	Complete dehalogenation in 24 h	54
Charge stabilized Ag and Au NPs (10–150 nm)	CCl_4, $C_6H_5CH_2Cl$, $CHCl_3$, CH_2Cl_2, *etc.*	Catalytic degradation	2-Propanol + water, 28 °C	AgCl, C and acetone	Complete destruction in 12 h	35
TiO_2 (40 and 80 nm)	CCl_4	Thermal decomposition	<550 °C, gaseous CCl_4	CO, CO_2, $COCl_2$, Cl_2, C, $TiCl_4$, HCl and titanium oxychloride	Particles of size 40 nm are more reactive than 80 nm	55
Monolayer-protected Ag clusters (<1 nm size)	CCl_4, $C_6H_5CH_2Cl$ and $CHCl_3$	Catalytic degradation	2-Propanol + water, 28 °C	AgCl, C, acetone and CCl_3COOH	Complete destruction within 3 h	Present study

$$Ag_9MSA_7(aq.) + (CH_3)_2CHOH + CCl_4 \rightarrow C + AgCl\downarrow + (CH_3)_2CO + 2H^+$$

B. Supported clusters. Clusters supported on neutral alumina were also used for the study of degradation of CCl_4. Reaction products were characterized by XRD, Raman and SEM EDAX. XRD (Fig. S5A†) confirms the formation of AgCl and Raman analysis (Fig. S5B†) reveals the presence of the carbonaceous material due to the degradation of halocarbon. EDAX analysis shows clearly the presence of Cl, Ag and S (Fig. S6†). The quantification table of elements also supports the formation of AgCl which shows the silver to chlorine atomic ratio as 1 : 1 (inset of Fig. S6†). Other halocarbons like $CHCl_3$ and $C_6H_5CH_2Cl$ were also degraded by unsupported and supported clusters giving silver chloride and amorphous carbon as the products (data are not shown). Time taken for complete destruction of $CHCl_3$ is comparable to the CCl_4 case, whereas for benzyl chloride, it was more. The possible reason is its complete immiscibility in the reaction mixture. XPS data of the reaction products of benzyl chloride and clusters are shown in Fig. 7A and B. A survey spectrum indicates the presence of elements C, O, Ag, S and Cl (Fig. 7A). The peak of Ag $3d_{5/2}$ at 367.7 eV confirms the presence of silver in the +1 oxidation state formed due to the reaction (Fig. 7B). The chemical change of the monolayer has been confirmed by the presence of S $2p_{3/2}$ at

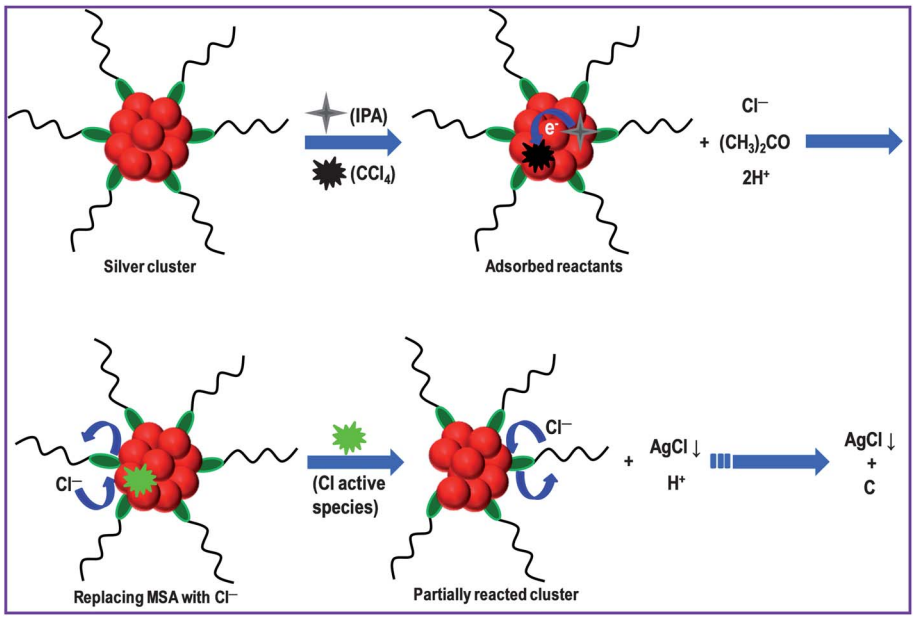

Scheme 1 Schematic representation of the degradation of halocarbon, CCl_4, by silver clusters along with other chemical transformations. All the chemical species detected are not marked.

168.5 eV (inset of Fig. 7A). The nature of Cl has been understood from the peak of Cl $2p_{3/2}$ at 198.2 (inset of Fig. 7A). This is due to Cl^- from AgCl. It is important to recall that as the reaction was complete in this case, no unreacted chlorine feature was detected.

It is good to compare the efficiency of degradation of halocarbons by quantum clusters with the corresponding nanoparticles. For that, the same quantities (25 mg) of clusters and nanoparticles were used for the degradation of 5 mL of CCl_4 under the same experimental conditions. Surprisingly, in the case of clusters, the color of the mixture disappeared after 1.5 h accompanied by the formation of a grey colored precipitate (Fig. 7C). But, in the case of nanoparticles, reddish black color turned to pale brown. No precipitate of AgCl was seen after 1.5 h, and CCl_4 remained at the bottom, as marked in Fig. 7b[1]. The color change reflects progress in the reaction. The color change and the presence of CCl_4 confirm that clusters are more efficient for the degradation reaction. Degradation of chlorocarbons by other relevant nanomaterials is compared in Table 1. This suggests that quantum clusters of silver are good candidates for efficient degradation of chlorocarbons. Other materials need light, high temperatures, *etc.* whereas in our study we show the possibility of degradation at room temperature by simple mixing.

Mechanism

We propose the following mechanism on the basis of experimental observations. After addition of IPA and CCl_4 to the cluster solution, adsorption of both would occur on the surface of the cluster. Clusters play two important roles: one in catalyzing the oxidation of IPA and the other in activating the halocarbon. Formation of acetone from IPA due to catalytic oxidation (on the surface of the cluster) has been confirmed by UV/Vis spectroscopic analysis during the reaction. The control experiment, *i.e.*, a mixture of clusters (in water) and IPA, reveals that there is no formation of acetone. Mixture of IPA and CCl_4 also does not lead to the formation of acetone with time. These observations clearly indicate the necessity of an electron acceptor for the facile formation of H^+ as indicated by the decrease in pH of the solution. Activation of the C–Cl bond of chlorocarbon may occur on the surface of the cluster as reported previously in the case of noble metals.[56] The electrons released in the oxidation of IPA are abstracted by activated CCl_4 on the surface leading to the formation of Cl^- and other active Cl species which may act as oxidizing agents. The Cl^- formed may replace some of the MSA ligands similar to a report wherein phenylethane thiolate on Au cluster was replaced by the halide ion.[57] As MSA is replaced by Cl^-, stability of the cluster is lost which makes silver to react to form crystalline AgCl. Once one Ag atom from a cluster is removed to form AgCl, the other silver atoms also take part in the reaction. The final pH of the reaction mixture is acidic which may also facilitate the mineralization of CCl_4. The molecules of the monolayer which are detached from the cluster surface will be oxidized in the solution to form stable sulphate/sulphite species (confirmed by XPS). The process is schematically represented in Scheme 1.

Summary and conclusions

In summary, we have studied the reaction of monolayer-protected atomically precise silver clusters and nanoparticles with halocarbons at room temperature. The presence of reaction products, silver chloride, CCl_3COO^- and amorphous carbon, was confirmed by various spectroscopic and microscopic tools. A possible mechanism for the reaction is proposed accounting for the observed products. The efficiency of clusters in degrading halocarbons is considerably higher than the corresponding nanoparticles. This was attributed to the smaller size and reduced nobility of silver. Control experiments and the measurement of pH were carried out to validate the proposed mechanism. A limitation of this material is the non-reusability. But the reaction product AgCl can be recovered and used to make metallic silver or silver clusters back again.

Acknowledgements

We thank the Department of Science and Technology (DST), Government of India, for constantly supporting our research program on nanomaterials. M.S.B. thanks the CSIR for a senior research fellowship.

References

1 R. Jin, *Nanoscale*, 2010, **2**, 343–362.
2 P. L. Xavier, K. Chaudhari, A. Baksi and T. Pradeep, *Nano Rev.*, 2012, **3**, 14767.
3 O. M. Bakr, V. Amendola, C. M. Aikens, W. Wenseleers, R. Li, N. L. Dal, G. C. Schatz and F. Stellacci, *Angew. Chem., Int. Ed.*, 2009, **48**, 5921–5926.
4 S. Kumar, M. D. Bolan and T. P. Bigioni, *J. Am. Chem. Soc.*, 2010, **132**, 13141–13143.
5 T. U. B. Rao and T. Pradeep, *Angew. Chem., Int. Ed.*, 2010, **49**, 3925–3929.
6 A. George, E. S. Shibu, S. M. Maliyekkal, M. S. Bootharaju and T. Pradeep, *ACS Appl. Mater. Interfaces*, 2012, **4**, 639–644.
7 M. Zhu, H. Qian, X. Meng, S. Jin, Z. Wu and R. Jin, *Nano Lett.*, 2011, **11**, 3963–3969.
8 Y. Lei, F. Mehmood, S. Lee, J. Greeley, B. Lee, S. Seifert, R. E. Winans, J. W. Elam, R. J. Meyer, P. C. Redfern, D. Teschner, R. Schloegl, M. J. Pellin, L. A. Curtiss and S. Vajda, *Science*, 2010, **328**, 224–228.
9 K.-I. Shimizu, R. Sato and A. Satsuma, *Angew. Chem., Int. Ed.*, 2009, **48**, 3982–3986.
10 M. M. A. Habeeb, P. K. Verma, S. K. Pal, A. Retnakumari, M. Koyakutty, S. Nair and T. Pradeep, *Chem.–Eur. J.*, 2010, **16**, 10103–10112.
11 Y. Lu and W. Chen, *Chem. Soc. Rev.*, 2012, **41**, 3594–3623.
12 M. M. A. Habeeb and T. Pradeep, *Chem. Phys. Lett.*, 2007, **449**, 186–190.
13 T. Udayabhaskararao, Y. Sun, N. Goswami, S. K. Pal, K. Balasubramanian and T. Pradeep, *Angew. Chem., Int. Ed.*, 2012, **51**, 2155–2159.
14 C. Kumara and A. Dass, *Nanoscale*, 2011, **3**, 3064–3067.

15 M. A. H. Muhammed, P. K. Verma, S. K. Pal, R. C. A. Kumar, S. Paul, R. V. Omkumar and T. Pradeep, *Chem.–Eur. J.*, 2009, **15**, 10110–10120.
16 M. S. Bootharaju and T. Pradeep, *Langmuir*, 2011, **27**, 8134–8143.
17 I. Chakraborty, T. Udayabhaskararao and T. Pradeep, *J. Hazard. Mater.*, 2012, **211–212**, 396–403.
18 Y. Liu, K. Ai, X. Cheng, L. Huo and L. Lu, *Adv. Funct. Mater.*, 2010, **20**, 951–956.
19 B. Schrick, J. L. Blough, A. D. Jones and T. E. Mallouk, *Chem. Mater.*, 2002, **14**, 5140–5147.
20 E. Sumesh, M. S. Bootharaju, Anshup and T. Pradeep, *J. Hazard. Mater.*, 2011, **189**, 450–457.
21 W. Zheng, J. Lichwa, M. D'Alessio and C. Ray, *Chemosphere*, 2009, **76**, 1167–1177.
22 C. Kroeze and L. Reijnders, *Sci. Total Environ.*, 1992, **112**, 269–290.
23 W.-Y. Xu and T.-Y. Gao, *J. Environ. Sci.*, 2007, **19**, 792–799.
24 G. W. Reynolds, J. T. Hoff and R. W. Gillham, *Environ. Sci. Technol.*, 1990, **24**, 135–142.
25 C. A. Keller, M. Hill, M. K. Vollmer, S. Henne, D. Brunner, S. Reimann, S. O'Doherty, J. Arduini, M. Maione, Z. Ferenczi, L. Haszpra, A. J. Manning and T. Peter, *Environ. Sci. Technol.*, 2011, **46**, 217–225.
26 C. E. Jones and L. J. Carpenter, *Environ. Sci. Technol.*, 2005, **39**, 6130–6137.
27 T.-K. Tseng, H. Chu and H.-H. Hsu, *Environ. Sci. Technol.*, 2002, **37**, 171–176.
28 Q. Xiang, J. Yu, B. Cheng and H. C. Ong, *Chem.–Asian J.*, 2010, **5**, 1466–1474.
29 X. Zhou, G. Liu, J. Yu and W. Fan, *J. Mater. Chem.*, 2012, **22**, 21337–21354.
30 O. Koper, I. Lagadic and K. J. Klabunde, *Chem. Mater.*, 1997, **9**, 838–848.
31 J. Farrell, M. Kason, N. Melitas and T. Li, *Environ. Sci. Technol.*, 1999, **34**, 514–521.
32 M. I. Litter, W. Choi, D. D. Dionysiou, P. Falaras, A. Hiskia, G. Li Puma, T. Pradeep and J. Zhao, *J. Hazard. Mater.*, 2012, **211–212**, 1–2.
33 I. V. Mishakov, V. I. Zaikovskii, D. S. Heroux, A. F. Bedilo, V. V. Chesnokov, A. M. Volodin, I. N. Martyanov, S. V. Filimonova, V. N. Parmon and K. J. Klabunde, *J. Phys. Chem. B*, 2005, **109**, 6982–6989.
34 C. L. Carnes and K. J. Klabunde, *Langmuir*, 2000, **16**, 3764–3772.
35 A. S. Nair and T. Pradeep, *Curr. Sci.*, 2003, **84**, 1560–1564.
36 A. S. Nair and T. Pradeep, *Indian Pat.*, 200767, 2006.
37 A. S. Nair and T. Pradeep, *U. S. Pat.*, 7,968,493B962, 2011.
38 A. S. Nair and T. Pradeep, *J. Nanosci. Nanotechnol.*, 2007, **7**, 1871–1877.
39 M. S. Bootharaju and T. Pradeep, *Langmuir*, 2012, **28**, 2671–2679.
40 T. Pradeep and Anshup, *Thin Solid Films*, 2009, **517**, 6441–6478.
41 E. S. Shibu and T. Pradeep, *Chem. Mater.*, 2011, **23**, 989–999.
42 T. U. B. Rao, B. Nataraju and T. Pradeep, *J. Am. Chem. Soc.*, 2010, **132**, 16304–16307.
43 R. John, A. Ashokreddy, C. Vijayan and T. Pradeep, *Nanotechnology*, 2011, **22**, 165701.
44 K. N. Kudin, B. Ozbas, H. C. Schniepp, R. K. Prud'homme, I. A. Aksay and R. Car, *Nano Lett.*, 2007, **8**, 36–41.
45 V. Palshin, E. I. Meletis, S. Ves and S. Logothetidis, *Thin Solid Films*, 1995, **270**, 165–172.
46 D. Fan, C. Zhang, J. He, R. Hua, Y. Zhang and Y. Yang, *J. Mater. Chem.*, 2012, **22**, 18564–18571.
47 M. S. Bootharaju and T. Pradeep, *J. Phys. Chem. C*, 2010, **114**, 8328–8336.
48 H. Zhang, Q. Fu, Y. Yao, Z. Zhang, T. Ma, D. Tan and X. Bao, *Langmuir*, 2008, **24**, 10874–10878.
49 H. Piao, K. Adib, Z. Chang, J. Hrbek, M. Enever, M. A. Barteau and D. R. Mullins, *J. Phys. Chem. B*, 2003, **107**, 13976–13985.
50 A. Henglein, B. G. Ershov and M. Malow, *J. Phys. Chem.*, 1995, **99**, 14129–14136.
51 K. D. Warren, R. G. Arnold, T. L. Bishop, L. C. Lindholm and E. A. Betterton, *J. Hazard. Mater.*, 1995, **41**, 217–227.
52 Y. Ukisu, S. Iimura and R. Uchida, *Chemosphere*, 1996, **33**, 1523–1530.
53 W. Choi and M. R. Hoffmann, *Environ. Sci. Technol.*, 1996, **31**, 89–95.
54 Y. Xu and W.-X. Zhang, *Ind. Eng. Chem. Res.*, 2000, **39**, 2238–2244.
55 G. Liu, J. Wang, Y. Zhu and X. Zhang, *Phys. Chem. Chem. Phys.*, 2004, **6**, 985–991.
56 H. Imai, T. Nishiguchi, M. Tanaka and K. Fukuzumi, *J. Org. Chem.*, 1977, **42**, 2309–2313.
57 M. Zhu, G. Chan, H. Qian and R. Jin, *Nanoscale*, 2011, **3**, 1703–1707.

